Retardation effects in atom-wall interactions

T. Das [1], C. A. Ullrich [2], and U. D. Jentschura [1]

[1]*Department of Physics and LAMOR, Missouri University of Science and Technology, Rolla, Missouri 65409, USA*

[2]*Department of Physics and Astronomy, University of Missouri, Columbia, Missouri 65211, USA*

(Received 6 October 2023; accepted 21 November 2023; published 15 February 2024)

The onset of retardation effects in atom-wall interactions is studied. It is shown that the transition range from the $1/z^3$ short-range (van der Waals) interaction to the $1/z^4$ long-range (Casimir) retarded interaction critically depends on the atomic properties and on the dielectric function of the material. For simple non-alkali-metal atoms (e.g., ground-state hydrogen and ground-state helium) interacting with typical dielectric materials such as intrinsic silicon, the transition to the retarded regime is shown to proceed at a distance of about 10 nm (200 Bohr radii). This is much shorter than typical characteristic absorption wavelengths of solids. Larger transition regimes are obtained for atoms with a large static polarizability such as metastable helium. We present a simple estimate for the critical distance, $z_{\rm cr} = 137\,\sqrt{\alpha(0)/Z}$ atomic units, where $\alpha(0)$ is the static polarizability (expressed in atomic units) and Z is the number of electrons of the atom.

DOI: 10.1103/PhysRevA.109.022808

I. INTRODUCTION

Dispersion forces between spatially well-separated microscopic systems are important for phenomena such as atom-surface scattering, physisorption, the structure of soft matter and two-dimensional layered materials, and many applications [1,2]. In this context, it is well known that atom-atom interactions undergo a transition from a short-range van der Waals ($1/R^6$) to a retarded long-range ($1/R^7$) behavior, where R is the interatomic distance (see Ref. [3] and Chaps. 4 and 11 of Ref. [4]). For atom-wall interactions, the asymptotic behavior changes from $1/z^3$ for short-range to $1/z^4$ in the long-range limit (see, e.g., Ref. [5]), due to a process called retardation. The interpolating formula has been given in Eqs. (18) and (21) of Ref. [6] (see also Ref. [7]). However, the precise nature of this transition is less well characterized in the literature. From Fig. 3 of Ref. [6], it is evident that the interaction of ^{87}Rb atoms with a sapphire surface starts to substantially deviate from the $1/z^3$ short-range asymptotics in the range $z \sim 30$ nm $\approx 600\,a_0$, where a_0 is the Bohr radius. For the example of metastable helium (in the triplet state) interacting with a gold surface, estimates for the transition region to the retarded regime have been indicated in the range of $z \leqslant 150$ nm $\approx 3000\,a_0$ in the text following Eq. (3) in Sec. III of Ref. [8], and in Secs. 16.3.4 and 16.4.2 of Ref. [9]. Here, we concentrate on metastable helium in the triplet $2\,^3S_1$ state, which has a radiative lifetime of about 7800 s and is thus sufficiently long-lived to probe atom-surface interactions in detail, including quantum reflection studies [10]. By contrast, while the $2\,^1S_0$ state also is metastable (dipole decay to the ground state is not allowed), its lifetime is much shorter, of the order of only 2×10^{-2} s. In this paper, we aim to provide clarity and give both simple estimates and precise numerical results that show the onset and spatial range of the transition regime between van der Waals and Casimir-Polder interactions. The dependence of the transition region on the atomic species and on the dielectric function of the surface is also studied.

Intuitively, we can understand the onset of retardation as follows: Atom-wall interactions happen due to the exchange of virtual photons. If an exchange photon picks up a non-negligible phase (of order unity) on its way from the atom to the wall and back, retardation needs to be taken into account (Chap. 5 of Ref. [4]). The phase of a characteristic photon is given as $\Delta\phi = k_{\rm ch} z$, where $k_{\rm ch}$ is the wave vector corresponding to a characteristic resonance excitation of the atom (or solid). The condition $\Delta\phi \sim 1$ leads to $z \sim 1/k_{\rm ch} = \lambda_{\rm ch}/(2\pi)$, where $\lambda_{\rm ch}$ is the characteristic wavelength. For simple atomic systems such as (atomic) hydrogen or helium (in their ground states), the characteristic excitation wavelength is $\lambda_{\rm ch} = \hbar c/E_h$, where $E_h = \alpha^2 mc^2$ is the Hartree energy (where α is the fine-structure constant, m is the electron mass, c is the speed of light, and the subscript h stands for Hartree). Hence, *a priori*, we can expect retardation effects to become important when the atom-wall distance is of the order of a Hartree wavelength λ_h,

$$z \sim \lambda_h = \frac{\hbar c}{E_h} = \frac{a_0}{\alpha} = 7.25\ \text{nm} = 137\ \text{a.u.}, \tag{1}$$

where a_0 is the Bohr radius, which is the unit of length in the atomic unit system. Throughout this article, we use the abbreviation a.u. for quantities given in atomic units. We note that λ_h is, purely parametrically, of the same order as optical wavelengths, but typical optical wavelengths in the visible spectrum are longer than λ_h; the ultraviolet spectrum ends at about 400 nm. Hence, one might ask whether or not large prefactors could shift the parametric estimate (1).

Here, we demonstrate that an extended distance scale for the nonretarded interaction may be observed for special atoms with an excessively large static polarizability, but that retardation sets in at much shorter length scales commensurate with Eq. (1) (in typical cases, about 10 nm $\approx$ 200 a.u.) for many simple atomic systems. For example, we demonstrate by explicit numerical calculations that the atom-wall interaction of ground-state helium atoms undergoes a transition to the

retarded regime much earlier, at length scales commensurate with $z \sim \lambda_h$. Variations of the onset of the retarded regime with the atomic system are also discussed.

This paper is organized as follows. We discuss the interpolating formula for the transition from the short-range to the long-range regime in Sec. II, with a special emphasis on interactions of hydrogen and helium with a silicon surface. Other elements are discussed in Sec. III. Atomic units are used throughout unless indicated otherwise [$\hbar = e = 1$, $\epsilon_0 = 1/(4\pi)$, $c = 1/\alpha$, where α is the fine-structure constant]. We provide mini-reviews of applicable distance ranges in Appendix A, parameters of our helium calculations in Appendix B, and parameters of the dielectric function of intrinsic silicon in Appendix C. A derivation of the Thomas-Reiche-Kuhn (TRK) sum rule for metastable reference states [11,12] is presented in Appendix D.

II. HYDROGEN AND HELIUM ON SILICON AND GOLD

We start from an interpolating expression for the atom-wall interaction, which reduces to the $1/z^3$ short-range interaction for small atom-wall distance and to the $1/z^4$ long-range interaction for a large distance. The relevant formula is given in Eqs. (18) and (21) of Ref. [6],

$$\mathcal{E}(z) = -\frac{\alpha^3}{2\pi} \int_0^\infty d\omega\, \omega^3\, \alpha(\mathrm{i}\omega) \int_1^\infty dp \mathrm{e}^{-2\alpha p \omega z} H(\epsilon(\mathrm{i}\omega), p), \tag{2}$$

where

$$H(\epsilon, p) = \frac{\sqrt{\epsilon - 1 + p^2} - p}{\sqrt{\epsilon - 1 + p^2} + p} + (1 - 2p^2) \frac{\sqrt{\epsilon - 1 + p^2} - p\epsilon}{\sqrt{\epsilon - 1 + p^2} + p\epsilon}. \tag{3}$$

Here, $\alpha(\mathrm{i}\omega)$ is the dynamic (dipole) polarizability of the atom at imaginary driving frequency, and $\epsilon(\mathrm{i}\omega)$ is the dielectric function of the solid at imaginary angular frequency. For the material of the solid (intrinsic silicon), we assume the interpolating model of the temperature-dependent dielectric function recently discussed in Ref. [13] for intrinsic silicon (with slight modifications). The parameters are reviewed in Appendix C. We also study gold, employing a simple plasma model for its dielectric function for definiteness and a modified model discussed in Eq. (13.46) of Ref. [9].

In the current section, we focus on atomic hydrogen and helium. For hydrogen, we employ the following formula for the dipole polarizability in the nonrecoil approximation (infinite nuclear mass), which is sufficient for the accuracy required in the current investigation,

$$\alpha_{\mathrm{H}}(\omega) = Q_{\mathrm{H}}(\omega) + Q_{\mathrm{H}}(-\omega), \tag{4}$$

where

$$Q_{\mathrm{H}}(\omega) = \frac{1}{3} \langle 1S | \vec{r}\, \frac{1}{H - E_{1S} + \hbar\omega}\, \vec{r} | 1S \rangle, \tag{5}$$

where E_{1S} is the ground-state energy of hydrogen, H is the Schrödinger-Coulomb Hamiltonian, and the scalar product is understood for the two position operators. According to Eq. (4.154) of Ref. [4], the dipole matrix element can be expressed as follows,

$$Q^{(\mathrm{H})}(\omega) = \frac{2t^2\, p(t)}{3\,(1-t)^5\,(1+t)^4} + \frac{256\, t^9\, f(t)}{3\,(1+t)^5\,(1-t)^5}, \tag{6}$$

where the photon energy is parametrized by the t variable, $t = t(\omega) = (1 + 2\omega)^{-1/2}$. The polynomial $p(t)$ incurred in Eq. (6) is

$$p(t) = 3 - 3t - 12t^2 + 12t^3 + 19t^4 - 19t^5 - 26t^6 - 38t^7. \tag{7}$$

The function $f(t)$ is a complete hypergeometric function,

$$f(t) = {}_2F_1(1, -t, 1 - t, \xi), \tag{8}$$

where $\xi = (1-t)^2/(1+t)^2$.

For helium, we use an approach based on a fully correlated basis set, using exponential basis functions [14–16]. We employ a Löwdin decomposition of the overlap matrix (see Appendix J of Ref. [17]) and use extended-precision arithmetic in the JULIA language [18–20] in order to avoid loss of numerical precision in intermediate steps of the calculation. The HTDQLS algorithm [21] is used to diagonalize the overlap matrix in arbitrary precision. Trial functions for S states are of the explicitly correlated form $\exp(-ar_1 - br_2 - cr_{12})$ with an appropriate symmetrization for particle interchange (positive sign for singlet states, negative sign for triplet states). Here, r_1 and r_2 are the distances of the two electrons from the helium nucleus, and r_{12} is the interelectron distance. For P states, trial functions are of the explicitly correlated form $x_1^i \exp(-ar_1 - br_2 - cr_{12})$, where $\vec{r}_1 = \sum_{i=1}^3 x_i \hat{e}_i$ in the Cartesian basis, again with an appropriate symmetrization for particle interchange. For the calculation of the matrix elements of the Hamiltonian, and the dipole transition matrix elements, one needs the master integrals given in Chap. 13 of Ref. [4]. Further details are relegated to Appendix B.

For the evaluation of the dynamic polarizability, two other approaches have been discussed in the literature, namely, the single-oscillator model [8,23] (henceforth referred to by the acronym 1osc) and the few-oscillator model [13] (henceforth referred to by the acronym fosc). The single-oscillator model, asymptotically matched to the static ($\omega \to 0$) and ultraviolet ($\omega \to \infty$) limits, reads as follows (in atomic units),

$$\alpha_{\mathrm{1osc}}(\mathrm{i}\omega) = \frac{Z}{\omega^2 + Z/\alpha(0)} = \frac{Z}{\omega^2 + \omega_{\mathrm{cr}}^2}. \tag{9}$$

Here, $\alpha(0)$ is the static polarizability, Z is the number of electrons, and the critical frequency is $\omega_{\mathrm{cr}} = \sqrt{Z/\alpha(0)}$ (this frequency will be important for our considerations in Sec. III). The formula (9) has the correct static limit [$\alpha(\mathrm{i}\omega = 0) = \alpha(0)$]. The correct ultraviolet limit is also obtained in view of the asymptotic relation $\alpha(\mathrm{i}\omega) \to Z/\omega^2$, which fulfills the TRK sum rule [11,12]. This sum rule remains valid for metastable reference states (see Appendix D). Values of $\alpha(0)$ have been tabulated in Ref. [24] for all elements with nuclear charge numbers $1 \leqslant Z \leqslant 120$. (Remark: It is also possible to match the single-oscillator model against the van der Waals coefficient of the atomic dimer system [25,26], but in this case, one fails to fulfill the TRK sum rule in the

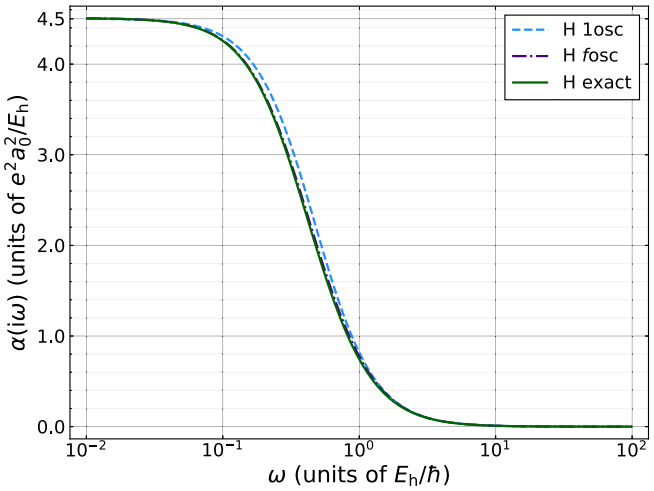

FIG. 1. Dynamic (dipole) polarizability of atomic hydrogen, $\alpha(\mathrm{i}\omega)$, as a function of the imaginary driving frequency. The exact values obtained from Eq. (4) are compared with the few-oscillator-strength-based model (fosc) described in Appendix B of Ref. [13]. The first 30 oscillator strengths and their corresponding transition energies are collected from Table 4 of Ref. [22] for the evaluation, which yields a maximum relative error of 4.16%. For comparison, the single-oscillator model, given in Eq. (9), is also plotted. The atomic polarizability is given in atomic units, i.e., in units of $e^2a_0^2/E_h$, where e is the electron charge, a_0 is the Bohr radius, and E_h is the Hartree energy.

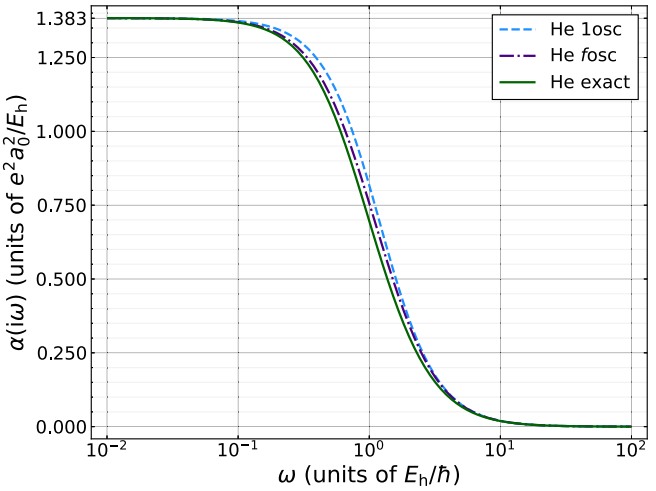

FIG. 2. Dynamic (dipole) polarizability of (ground-state) atomic helium as a function of imaginary driving frequency. The values obtained from the exact approach based on a fully correlated basis set are compared with the oscillator-strength-based model. Oscillator strengths for excited states from $n = 2$ to $n = 10$, and their corresponding transition energies are collected from Table 14 of Ref. [22] for the evaluation, which yields a maximum relative error of 12.14%. For comparison, the single-oscillator model [Eq. (9)] is also plotted.

ultraviolet region. Here, we use the functional form given in Eq. (9).)

As an intermediate between the exact calculation of the dynamic polarizability and the single-oscillator model, the few-oscillator model has recently been discussed in Appendix B of Ref. [13]. Let us assume that a finite number of oscillator strengths f_n are known ($n \in \{1, \ldots, N\}$), with corresponding resonance frequencies ω_n. The few-oscillator strength model reads as follows,

$$\alpha_{\mathrm{fosc}}(\mathrm{i}\omega) = \sum_{n=1}^{N} \frac{f_n}{\omega^2 + \omega_n^2} + \frac{1}{\omega^2 + \omega_c^2}\left(Z - \sum_{n=1}^{N} f_n\right), \quad \text{(10a)}$$

$$(\omega_c)^2 = \frac{Z - \sum_{n=1}^{N} f_n}{\alpha(0) - \sum_{m=1}^{N} f_m/\omega_m^2}. \quad \text{(10b)}$$

Here, ω_c describes the typical scale of virtual excitations into the continuum. One collects a number N of oscillator strengths [first term on the right-hand side of Eq. (10a)] and approximates the completion of the spectrum by including the second term on the right-hand side of Eq. (10a). The choice of the frequency ω_c in Eq. (10b) ensures that the correct static limit $\alpha(0)$ is reproduced. From tables (e.g., Ref. [22]), it is possible to collect at least $N = 9$ oscillator strengths to the lowest excited states for typical atomic species.

In Figs. 1 and 2, and Fig. 3 for metastable helium, we show that the oscillator-strength-based approach used in Ref. [13], which is enhanced by matching the static polarizability and the ultraviolet limits with accurate limits, yields numerical data for the dynamic polarizability of hydrogen and helium which are in good agreement with the exact results.

A comparison of the single-oscillator model to the few-oscillator–strength model illustrates the gradual improvement achieved by including more known oscillator strengths. Another observation is as follows: The presence of resonances due to transitions to other bound-state energy levels has a tendency to lower the curve of $\alpha(\mathrm{i}\omega)$ upon the inclusion of more bound-state resonances as compared to the single-oscillator model, i.e., one has $\alpha_{\mathrm{1osc}}(\mathrm{i}\omega) > \alpha_{\mathrm{fosc}}(\mathrm{i}\omega) > \alpha(\mathrm{i}\omega)$. Hence, the single-oscillator model tends to overestimate the polarizability at finite excitation frequencies, while reproducing the correct limit for very high frequencies.

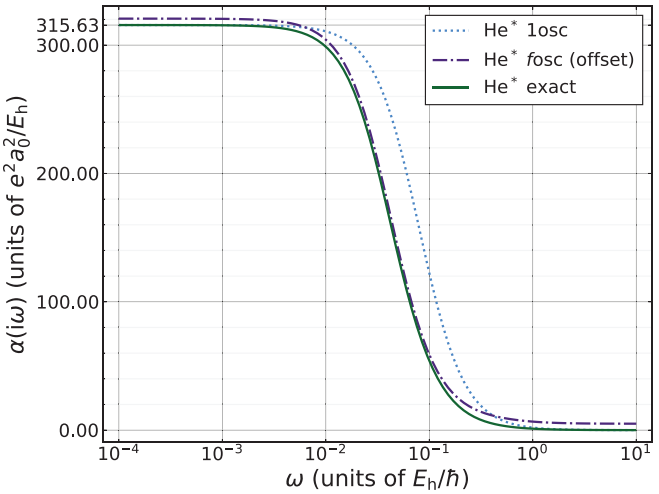

FIG. 3. Same as Figs. 1 and 2, but for metastable helium (He*) in the $2\,^3S_1$ reference state. Because the two curves for the fosc model and the exact polarizability almost overlap, the curve for the fosc model is shifted upwards by a constant offset of +5.0 a.u. in order to make the curves visually discernible.

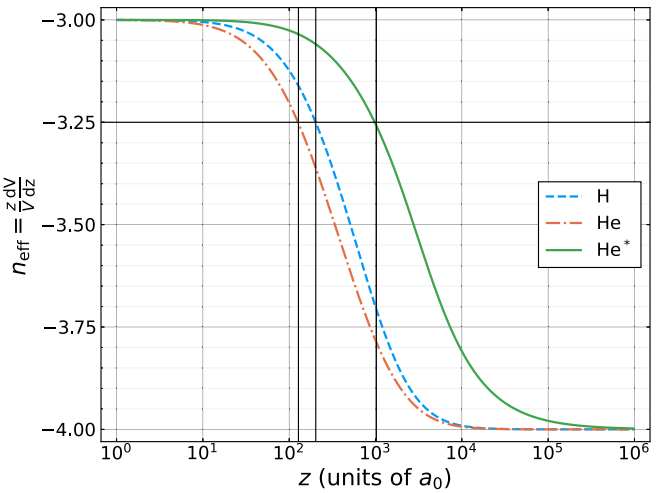

FIG. 4. Change in the effective exponent $n_{\rm eff}$ for atom-wall interactions due to the transition from the short-range (van der Waals) to the long-range (Casimir) regime for hydrogen, ground-state helium, and metastable $2\,^3S_1$ helium, interacting with intrinsic silicon. To this end, the atom-wall potential is numerically evaluated and the effective exponent is calculated via Eq. (11) as a function of the atom-wall separation. The Clausius-Mossotti (CM) model described in Ref. [13] is used for the dielectric function of intrinsic silicon, with slightly modified parameters (see Table I). The exact dynamic polarizability is used for all atoms.

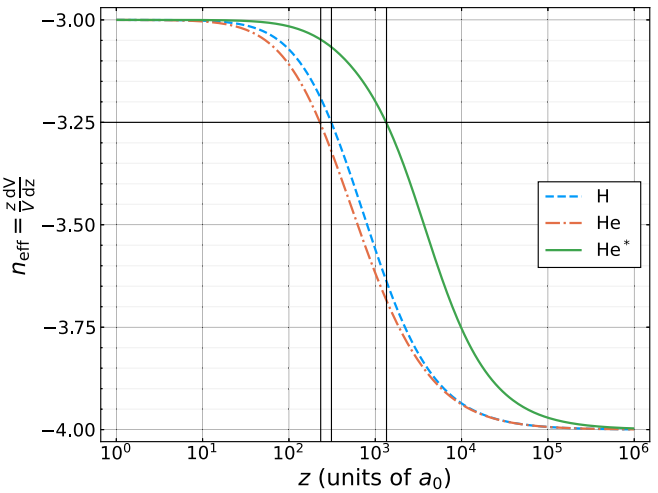

FIG. 5. Breakdown of the short-range asymptotics for the atom-wall interaction for hydrogen interacting with gold, as described by the plasma model (14). Otherwise, the figure is analogous to Fig. 4.

In order to gauge the transitions from the short-range to the long-range regime, we use the effective "local" power coefficient

$$n_{\rm eff} = \frac{z}{V(z)}\frac{dV(z)}{dz} = \frac{d\ln(|V(z)|)}{d\ln(z)}. \tag{11}$$

It evaluates to exactly n when $V(z) = V_0 z^n$. By the logarithm of the potential, we understand the logarithm of the numerical value (reduced quantity) of the potential, expressed in atomic units.

The dependence of the effective exponent $n_{\rm eff}$ on the atom-wall distance z is shown in Figs. 4 and 5 for the interaction of H, He, and H* with silicon and gold, respectively. Let us define the breakdown point $z_{\rm br}$ for the short-range expansion to be the distance where the effective exponent $n_{\rm eff}$ reaches the value $n_{\rm eff} = -3.25$, which is 25% of the way between the asymptotic short-range value ($n_{\rm eff} = -3$) and the long-range value ($n_{\rm eff} = -4$). This definition, while arbitrary to some extent, captures the essence of the transition between the two regimes. In addition to the substantial deviation of the effective exponent $n_{\rm eff}$ from the value $n_{\rm eff} = -3$ at the breakdown point, we have checked that the relative deviation of the atom-surface potential $V(z)$ from the short-range estimate (19), parametrized by the function $D(z) = [V(z) - (-C_3/z^3)]/V(z)$, is at least 35 % at $z = z_{\rm br}$, further validating the sensibility of our definition.

From Fig. 4, one reads off the following values for interactions with intrinsic silicon:

$$z_{\rm br}({\rm H};{\rm Si}) \approx 203\ {\rm a.u.}, \tag{12a}$$

$$z_{\rm br}({\rm He};{\rm Si}) \approx 126\ {\rm a.u.}, \tag{12b}$$

$$z_{\rm br}({\rm He}^*;{\rm Si}) \approx 1033\ {\rm a.u.} \tag{12c}$$

When using the single-oscillator model, the values change into

$$z_{\rm br}({\rm H};1{\rm osc};{\rm Si}) \approx 194\ {\rm a.u.}, \tag{13a}$$

$$z_{\rm br}({\rm He};1{\rm osc};{\rm Si}) \approx 117\ {\rm a.u.}, \tag{13b}$$

$$z_{\rm br}({\rm He}^*;1{\rm osc};{\rm Si}) \approx 674\ {\rm a.u.} \tag{13c}$$

For the fosc model, the values of $z_{\rm br}$ are in between the values for the exact polarizabilities and those for the 1osc model, namely, 200, 121, and 1005 a.u., respectively, for H, He, and He*.

Another example is the calculation of $z_{\rm br}$ for interactions with gold, where we use the plasma model,

$$\epsilon(i\omega) = 1 + \frac{\omega_{\rm pl}^2}{\omega^2}, \tag{14}$$

where $\omega_{\rm pl}$ is the plasma frequency. For the plasma frequency $\omega_{\rm pl}$, we use the same value as advocated in Ref. [9], namely, 9 eV. The dielectric function of the plasma model diverges in the limit $\omega \to 0$, which implies that the long-range limit of the interaction with a gold surface is the same as that for a perfect conductor (see also Ref. [7]). The dielectric function of gold, approximated by the plasma model, is strongly peaked for very low frequency; it constitutes a cursory approximation. Because of the strong emphasis on very low virtual photon frequencies, we can expect $z_{\rm br}$ to be exceptionally large as compared to other materials (see also the discussion in Sec. III).

Figure 5 shows the breakdown of the short-range expansion for hydrogen and ground-state and metastable helium, for interactions with gold. One reads off the values

$$z_{\rm br}({\rm H};{\rm Au}) \approx 309\ {\rm a.u.}, \tag{15a}$$

$$z_{\rm br}({\rm He};{\rm Au}) \approx 228\ {\rm a.u.}, \tag{15b}$$

$$z_{\rm br}({\rm He}^*;{\rm Au}) \approx 1414\ {\rm a.u.} \tag{15c}$$

For the single-oscillator model, one obtains

$$z_{\rm br}({\rm H};\,1{\rm osc};\,{\rm Au}) \approx 297\ {\rm a.u.}, \tag{16a}$$

$$z_{\rm br}({\rm He};\,1{\rm osc};\,{\rm Au}) \approx 217\ {\rm a.u.}, \tag{16b}$$

$$z_{\rm br}({\rm He}^*;\,1{\rm osc};\,{\rm Au}) \approx 892\ {\rm a.u.} \tag{16c}$$

For the fosc model, the values of $z_{\rm br}$ are in between the values for the exact polarizabilities and those for the 1osc model, namely, 306, 223, and 1399 a.u., respectively, for H, He, and He*.

The breakdown distance depends quite substantially on the atomic system. These observations raise the question of the general dependence of the breakdown of the short-range expansion on the atomic species and on the properties of the solid.

We have already mentioned that the plasma model of gold leads to exceptionally large values of $z_{\rm br}$. This can be ramified: For example, the modified plasma model given in Eq. (13.46) of Ref. [9] adds additional terms which modify the plasma model given in Eq. (14) for higher frequencies, while the leading asymptotics for $\omega \to 0$ are unmodified. The addition of further terms shifts the dominant contribution to the integrals to higher frequencies ω, mimicking larger values of $\omega_{\rm cr}$ and leading to smaller values of $z_{\rm br}$. [One notices that $\omega_{\rm cr}$ is proportional to $\sqrt{Z/\alpha(0)}$, while $z_{\rm br}$ can be estimated to be proportional to $\sqrt{\alpha(0)/Z}$, according to Eq. (21).] This is indeed confirmed. When using the exact polarizabilities and the modified plasma model given in Eq. (13.46) of Ref. [9], the results given in Eq. (15) change into 201, 123, and 1311 a.u., respectively, for H, He, and He*. The relative change as compared to the simple plasma model given in Eq. (14) is smallest for metastable helium; this is due to emphasis on smaller excitation frequencies (small value of $\omega_{\rm cr}$ for metastable helium, see Fig. 3), where the simple plasma model given in Eq. (14) and the modified plasma model given in Eq. (13.46) of Ref. [9] share the same asymptotics.

III. OTHER ELEMENTS

The question of the dependence of the breakdown distance $z_{\rm br}$ on the atomic species is made more urgent by the observation that more complex atoms with occupied inner shells typically have a much larger static polarizability [24] and much smaller typical excitation energies (at least to the first excited states, see Ref. [27] for a compilation). One might think that the smaller (lowest) excitation energies of more complex atoms could imply a much narrower functional form of the dynamic polarizability $\alpha({\rm i}\omega)$ for more complex atoms and, hence, a drastic extension of the nonretarded $1/z^3$ short-range regime. However, one could also counterargue that more complex atoms also possess transitions to much higher excited states. Hence, one could argue that these higher-energy virtual transitions might lower the distance range for the onset of retardation.

The discussion of other atomic species is made easier by investigating the general structure of the atom-surface interaction integral given in Eq. (2). In order to estimate how far the nonretarded approximation is valid, let us start from the regime of not excessively large z. In this case, the exponential suppression factor $\exp(-\alpha\omega pz)$ is not very pronounced, and the dominant integration region comes from large p. We expand $H[\epsilon({\rm i}\omega),\,p]$ for large p with the result,

$$H[\epsilon({\rm i}\omega),\,p] \approx 2p^2\,\frac{\epsilon({\rm i}\omega)-1}{\epsilon({\rm i}\omega)+1}, \tag{17}$$

commensurate with the leading term recorded in Eq. (22) of Ref. [28]. One then carries out the integral over p in Eq. (2) and obtains the approximate formula

$$\mathcal{E}(z) \approx -\frac{1}{4\pi z^3}\int_0^\infty e^{-2\,\alpha\,\omega\,z}\alpha({\rm i}\omega)\,\frac{\epsilon({\rm i}\omega)-1}{\epsilon({\rm i}\omega)+1}. \tag{18}$$

Now, if one can ignore the exponential suppression factor $\exp(-2\alpha\omega z)$ over the entire characteristic ω integration region, then one can approximate the interaction energy by the very simple expression

$$\mathcal{E}(z) \approx -\frac{1}{4\pi z^3}\int_0^\infty \alpha({\rm i}\omega)\,\frac{\epsilon({\rm i}\omega)-1}{\epsilon({\rm i}\omega)+1} = -\frac{C_3}{z^3}, \tag{19}$$

where C_3 is defined in the obvious way. This is precisely the short-range asymptotic limit [in the expansion in powers of z and $\ln(z)$] of the atom-surface interaction energy. The term given in Eq. (19) corresponds to the expression $-C_3/z^3$; the leading short-range C_3 coefficient is otherwise listed in Eq. (35) of Ref. [28] (it is called C_{30} in Ref. [28]) and in Eq. (16.24) of Ref. [9]. However, if one cannot ignore the exponential suppression (retardation) factor $\exp(-2\,\alpha\,\omega\,z)$ over the relevant characteristic ω integration region, then the short-range expansion breaks down, and the atom-surface interaction energy is no longer well approximated by Eq. (19). We can thus conclude that the nonretardation approximation is valid in the distance range

$$z \lesssim \frac{1}{\alpha\,\omega_{\rm ch}}, \tag{20}$$

where $\omega_{\rm ch}$ is the *largest* characteristic frequency in the problem, i.e., either in the polarizability or in the dielectric function of the material.

The *largest* characteristic excitation frequency will typically be obtained from the atom, not from the solid. Typical characteristic excitation energies for solids are in the range of a few eV, as is evident from the extensive tabulation of dielectric functions in Ref. [29]. For conductors whose dielectric function is described by the plasma model given in Eq. (14), the characteristic absorption frequency is zero. This is evident if one writes the expression for the plasma model dielectric function as $1+\omega_{\rm pl}^2/(\omega^2+\omega_0^2)$ with $\omega_0 = 0$.

Let us use the single-oscillator model and define the *critical* distance $z_{\rm cr}$ for the onset of retardation effects to be the scale where the condition (20) breaks down. This means that the critical angular frequency and its corresponding distance scale (in atomic units) are respectively

$$\omega_{\rm cr} = \sqrt{\frac{Z}{\alpha(0)}}\ {\rm a.u.}, \quad z_{\rm cr} = 137\sqrt{\frac{\alpha(0)}{Z}}\ {\rm a.u.} \tag{21}$$

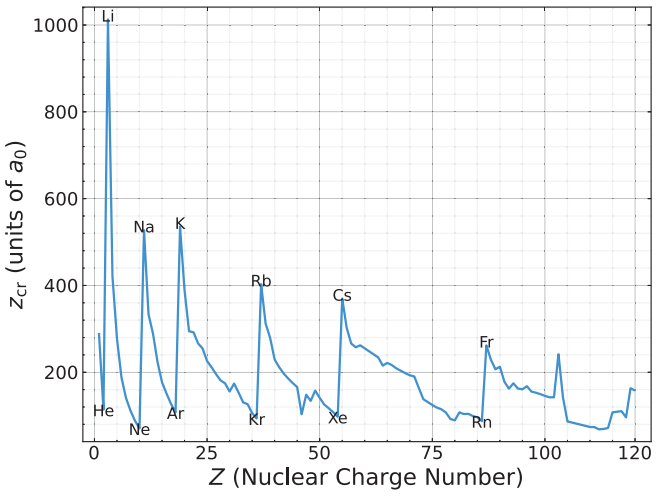

FIG. 6. Critical distance z_{cr} versus nuclear charge number Z, for all elements with $1 \leqslant Z \leqslant 120$ given in Ref. [24].

The estimates from Eq. (21) read as follows (using data from Ref. [24]):

$$z_{cr}(\mathrm{H}) = 137\sqrt{\frac{4.5}{1}}\ \text{a.u.} = 290\ \text{a.u.}, \tag{22a}$$

$$z_{cr}(\mathrm{He}) = 137\sqrt{\frac{1.383}{2}}\ \text{a.u.} = 113\ \text{a.u.}, \tag{22b}$$

$$z_{cr}(\mathrm{He}^*) = 137\sqrt{\frac{316}{2}}\ \text{a.u.} = 1720\ \text{a.u.} \tag{22c}$$

The correspondence (in terms of the order-of-magnitude) $z_{cr}(\mathrm{H}) \sim z_{br}(\mathrm{H})$, $z_{cr}(\mathrm{He}) \sim z_{br}(\mathrm{He})$, and $z_{cr}(\mathrm{He}^*) \sim z_{br}(\mathrm{He}^*)$, is obvious. In the latter case, the order-of-magnitude approximation $z_{cr}(\mathrm{He}^*)$ is larger than $z_{br}(\mathrm{He}^*)$ by about 27 %, which is perfectly acceptable given the cursory nature of the approximation. A plot of values of z_{cr} for all elements with $1 \leqslant Z \leqslant 120$ is presented in Fig. 6. Peak values are observed for alkali metals, which typically display a very large static polarizability.

For the case studied here, we have $z_{cr} > z_{br}$; i.e., the onset of retardation happens a bit earlier than predicted by the approximation $z \approx z_{cr}$. At $z = z_{cr}$, we have

$$\exp(-2\alpha\omega_{cr}\, z_{cr}) = [\exp(1)]^{-2} = 0.135, \tag{23}$$

indicating that, for typical excitation frequencies $\omega \sim \omega_{cr}$, the exponential suppression of the integrand in Eq. (18) is already very substantial at $z = z_{cr}$. This fact supports the observation that $z_{br} < z_{cr}$. Still, the approximation $z_{br} \approx z_{cr}$ remains a good, albeit somewhat cursory, estimate for the transition to the retarded regime.

IV. CONCLUSIONS

The world of atomic physics is full of surprises in terms of nonparametric prefactors. An example is the variation of the static polarizability with the atomic species (element number). Parametrically, the static polarizabilities of all atoms are of order $e^2a_0^2/E_h$, where e is the electron charge, a_0 is the Bohr radius, and E_h is the Hartree energy. However, large nonparametric prefactors multiply this estimate, two extreme cases being metastable triplet $2\,^3S_1$ helium, with a static polarizability of 315 a.u., and lithium, with a static polarizability of 164 a.u.

Another surprise, not treated here in further detail, is the large static polarizability of metastable singlet $2\,^1S_0$ helium, which amounts to about 800 a.u. However, atomic polarizabilities are not the only quantities leading to surprises. As an example in a different context, the so-called relativistic Bethe logarithm for S states of hydrogen, parametrically, was estimated to be of the order of $\alpha(Z\alpha)^4E_h$. After considerable efforts by a number of groups [30–34], a surprising nonparametric prefactor ≈ -31 (for nuclear charge number $Z = 1$) was confirmed to multiply the parametric estimate, shifting theoretical predictions for the Lamb shift of the ground state of hydrogenlike bound systems [30–35]. Furthermore, the nonlogarithmic prefactor was seen to remain numerically large (in between -28 and -31) for nuclear charge numbers $1 \leqslant Z \leqslant 5$. In order to appreciate the large magnitude of the nonlogarithmic correction to the Lamb shift, one observes that the relativistic Bethe logarithm (nonlogarithmic) correction of order for the ground state of hydrogenlike boron (nuclear charge number $Z = 5$) almost doubles the effect of the leading double logarithm $-\alpha(Z\alpha)^4E_h\,\ln^2[(Z\alpha)^{-2}]$, as is evident from Eq. (3) and Table I of Ref. [35].

Within the context of atom-wall interactions, we can expect the nonretarded regime to extend furthest for those atoms with the highest static polarizabilities at the lowest nuclear charge numbers. Indeed, we have demonstrated that the onset of retardation in atom-wall interactions depends quite significantly on the atomic species, even if, parametrically, the estimate (1) remains valid for all. For simple atomic systems such as hydrogen and ground-state helium, retardation effects set in already at distances of less than 10 nm $\approx$ 200 a.u. in atom-wall interactions. This result is consistent with remarks in the text following Eq. (2.16) of Ref. [36]. The breakdown of the short-range $1/z^3$ approximation happens at distance scales indicated in Eqs. (12), (15), and (22). An explicit estimate, $z_{cr} = 137\,(\alpha(0)/Z)^{1/2}$ a.u., was given in Eq. (21).

With the exception of lithium (and metastable helium), the critical distance for the onset of retardation effects does not exceed 600 a.u., as shown in Fig. 6. An exceptional example is provided by metastable helium where z_{cr} assumes the exceptionally large value of 1720 a.u., in view of an exceptionally large static polarizability of 315.63 a.u. However, the actual breakdown distance for metastable helium is smaller, namely, 1033 and 1414 a.u. for interactions with silicon and gold, respectively (the latter being described by a simple plasma model).

We can thus confirm that comparatively large z_{br} can be expected for metastable helium, especially for interactions with very good conductors, an extreme example being provided by the plasma model (14) for gold. However, even in this extreme case, the nonretarded regime is limited to about 1400 a.u. We conclude that the short-range approximation, for atom-wall interactions, breaks down much earlier than for solid-solid interactions [9] and we provide estimates for all elements in the periodic table (see Fig. 6).

ACKNOWLEDGMENTS

Helpful conversations with M. DeKieviet and C. Moore are gratefully acknowledged. T.D. and U.D.J. were supported by NSF Grant No. PHY–2110294. C.A.U. acknowledges support from NSF Grant No. DMR–2149082.

APPENDIX A: DEFINITION OF DISTANCE RANGES

The designations of "short-range" and "long-range" asymptotics crucially depend on the point of view. Because the designations are not always consistent, we here present a mini-review of this issue.

Zaremba and Kohn [37] define "close range" to be the range of a few atomic radii, commensurate with their aim to study the transition from physisorption to the van der Waals regime; the latter is understood as the "long-range regime" in Ref. [37].

On the other hand, Antezza *et al.* [6] define the "long-range regime" as the limit of very large separations far beyond the validity of van der Waals and Casimir-Polder interactions. This limit is characterized by a very-long range nonretarded tail proportional to $1/z^3$, which is due to effects described by thermal field theory (contributions of the first Matsubara frequency), and vanishes at zero temperature. The numerical coefficient of this extreme $1/z^3$ long-range tail is very small (see Eq. (17) of Ref. [6]) and we do not consider it here.

Thus, from the viewpoint of Ref. [6], the extreme short range is the regime of less than ten atomic radii, where the discretization of the crystal surface starts to play a role. The short-range regime is the $1/z^3$ nonretarded (van der Waals) range. The $1/z^4$ Casimir-Polder interactions then define the long-range regime. This is the viewpoint we also adopt in the present paper.

For completeness, let us also say a few words about the limit of very close approach to the surface. Zaremba and Kohn [37] showed that in this limit the van der Waals interaction becomes $-C_3/(z-z_0)^3$, where z_0 is a parameter, of order unity in atomic units, which can be calculated separately or obtained experimentally. For dielectric solids, the position of the reference plane is well approximated by $z_0 \approx d/2$, where d is the distance between layers of the substrate [36,38].

In other investigations [38,39], van der Waals-corrected density-functional theory (DFT) is used in order to calculate the adsorption energies of atoms on surfaces (e.g., rare gases on noble metals). The quadrupole correction is routinely taken into account in this procedure (see Table III of Ref. [38] and Ref. [7]), and the van der Waals energy is added to the contact energy at the equilibrium position of the atom in the immediate vicinity of the surface, the latter being calculated with the use of DFT (see Table III of Ref. [38] and also Ref. [40] for a general discussion of van der Waals-corrected DFT). This procedure is consistent with remarks made after Eq. (2.39) of Ref. [37], where the authors stress that their approach should be valid for the region of physisorption (i.e., for the range in between 4 and 7 a.u.).

APPENDIX B: PARAMETERS OF THE HELIUM CALCULATION

The a, b, and c parameters of the exponential basis functions $\exp(-ar_1 - br_2 - cr_{12})$ set are chosen in the same way for the reference ground state and the triple metastable excited reference state. One notes that our choice is different from, say, the basis set indicated in Eq. (18) of Ref. [41]. Through experimentation, we found it numerically favorable to implement a linear dependence of the exponents of the basis functions in the exponential basis with the index of the function.

Specifically, we use a Cartesian approach [42] and write the following expressions for the singlet ^1S, triplet ^3S, singlet ^1P, and triplet ^3P states,

$$\psi_{n\,^1\mathrm{S}}(\vec{r}_1,\vec{r}_2) = \sum_{j=1}^{j_{\max}} c_{n\,^1\mathrm{S},j}\, f_{n\,^1\mathrm{S},j}(r_1,r_2,r_{12}), \tag{B1a}$$

$$f_{n\,^1\mathrm{S},j}(r_1,r_2,r_{12}) = \exp(-a_j r_1 - b_j r_2 - c_j r_{12}) + \exp(-b_j r_1 - a_j r_2 - c_j r_{12}), \tag{B1b}$$

$$\psi_{n\,^3\mathrm{S}}(\vec{r}_1,\vec{r}_2) = \sum_{j=1}^{j_{\max}} c_{n\,^3\mathrm{S},j}\, f_{n\,^3\mathrm{S},j}(r_1,r_2,r_{12}), \tag{B1c}$$

$$f_{n\,^3\mathrm{S},j}(r_1,r_2,r_{12}) = \exp(-a_j r_1 - b_j r_2 - c_j r_{12}) - \exp(-b_j r_1 - a_j r_2 - c_j r_{12}), \tag{B1d}$$

$$\psi^i_{n\,^1\mathrm{P}}(\vec{r}_1,\vec{r}_2) = \sum_{j=1}^{j_{\max}} c_{n\,^1\mathrm{P},j}\, f^i_{n\,^1\mathrm{P},j}(r_1,r_2,r_{12}), \tag{B1e}$$

$$f^i_{n\,^1\mathrm{P},j}(r_1,r_2,r_{12}) = x_1^i \exp(-a_j r_1 - b_j r_2 - c_j r_{12}) + x_2^i \exp(-b_j r_1 - a_j r_2 - c_j r_{12}), \tag{B1f}$$

$$\psi^i_{n\,^3\mathrm{P}}(\vec{r}_1,\vec{r}_2) = \sum_{j=1}^{j_{\max}} c_{n\,^3\mathrm{P},j}\, f^i_{n\,^3\mathrm{S},j}(r_1,r_2,r_{12}), \tag{B1g}$$

$$f^i_{n\,^3\mathrm{P},j}(r_1,r_2,r_{12}) = x_1^i \exp(-a_j r_1 - b_j r_2 - c_j r_{12}) - x_2^i \exp(-b_j r_1 - a_j r_2 - c_j r_{12}). \tag{B1h}$$

The $c_{n\,^{2S+1}L,j}$ coefficients depend on the principal quantum number n, the total spin S, and the total orbital angular momentum L. The basis states $f_{n\,^{2S+1}L,j}(r_1,r_2,r_{12})$ multiply the coefficients. Within the manifold of states of specified symmetry, one calculates the Hamiltonian matrix within the basis spanned by $f_{n\,^{2S+1}L,j}(r_1,r_2,r_{12})$, and the overlap matrix of the same basis states, using the approach outlined in Ref. [41] and Chap. 13 of Ref. [4]. Let now $\mathbb{S}_{jj'} = \langle j|j'\rangle$ be the overlap matrix and $\mathbb{H}_{jj'} = \langle j|H_{\mathrm{NR}}|j'\rangle$, where H_{NR} is the Schrödinger Hamiltonian of helium in the nonrelativistic approximation (see Chap. 13 of Ref. [4]). The diagonalization of the effective Hamiltonian $\mathbb{H}_{\mathrm{eff}} = \mathbb{S}^{-1/2}\,\mathbb{H}\,\mathbb{S}^{-1/2}$ leads to discrete states; the first of which describe low-lying bound states, while the higher excited states with positive-energy eigenvalues above the ionization threshold serve to describe the continuum spectrum, in terms of a pseudospectrum of discrete states. The summation over j goes from $j=1$ to $j_{\max}$, where a value of $j_{\max} = 512$ turns out to be fully sufficient for our purposes here. Let us relate the summation index $j = (n_{\max})^3$ to three summation indices, k, ℓ, and m, all of which go from 1 to

$n_{\max} = 8$ (in our calculation),

$$k \in \{1, \ldots, n_{\max}\}, \qquad \ell \in \{1, \ldots, n_{\max}\}, \tag{B2a}$$

$$m \in \{1, \ldots, n_{\max}\}, \qquad j_{\max} = (n_{\max})^3, \tag{B2b}$$

$$j = k - 1 + n_{\max}(\ell - 1) + (n_{\max})^2(m - 1) + 1. \tag{B2c}$$

This generates a basis of $(n_{\max})^3$ functions. The relations (B2) define a unique mapping $(k, \ell, m) \leftrightarrow j$. Given j, one can calculate $k = k(j)$, $\ell = \ell(j)$, and $m = m(j)$, using $m = \{j - \mathrm{mod}[j-1, (n_{\max})^2] - 1\}/(n_{\max})^2 + 1$, $\ell = \{j - (m-1)(n_{\max})^2 - \mathrm{mod}[j - (m-1)(n_{\max})^2 - 1, n_{\max}] - 1\}/n_{\max} + 1$, and $k = j - (m-1)(n_{\max})^2 - (\ell - 1)\, n_{\max}$. The parameters are chosen to depend linearly on k, ℓ, and m, in such a way as to avoid degeneracies in the basis (hence using prime numbers),

$$a_j = a_{k(j)} = \frac{\sqrt{3}}{10}\,(k+1), \tag{B3a}$$

$$b_\ell = b_{\ell(j)} = \frac{9\,(\sqrt{17} - \sqrt{5})}{100}\,(\ell + 1), \tag{B3b}$$

$$c_m = c_{m(j)} = \frac{1}{10}\,(m+1). \tag{B3c}$$

This choice involves basis functions of the type $\exp(-ar_1 - br_2 - cr_{12})$ with numerically large coefficients $a = a_k$, $b = b_\ell$, and $c = c_k$, achieved for $k, \ell, m = n_{\max}$. Consequently, steep exponential decay is realized for some of the basis functions, which is helpful in a suitable description of the region near the cusp, $r_{12} = 0$. For low values of k, ℓ, and m, we achieve a good sampling of the large-distance region, which is important for a good description of oscillator strengths.

With very modest computational effort, this approach reproduces other data [41,43–46] for low-lying energy levels of helium, and for the static and dynamic polarizability of helium (within the nonrelativistic approximation), to better than 1 per mille [47]. Specifically, we obtain a value of 1.383 192 a.u. for the ground-state static polarizability, which compares well with Refs. [46,47], and an oscillator strength of 0.276 167 a.u. for the $1\,^1S$–$2\,^1P$ oscillator strength, which compares well with Ref. [46]. For the static polarizability of the metastable triplet state, we obtain a value of 315.63 a.u., which compares well with Ref. [24]. For the $2\,^3S$–$2\,^3P$ oscillator strength, we obtain a value of 0.5391 a.u., which compares well with Ref. [48].

APPENDIX C: INTRINSIC SILICON

In this Appendix, we provide a brief review of the Clausius-Mossotti fits recently employed in Ref. [13] for intrinsic silicon. We also take the opportunity to correct a few typographical errors. From Ref. [13], we recall the Lorentz-Dirac master function as follows:

$$f(T_\Delta, \omega) = \sum_{k=1}^{k_{\max}} \frac{a_k\big(\omega_k^2 - \mathrm{i}\gamma_k'\omega\big)}{\omega_k^2 - \omega^2 - i\omega\gamma_k}, \tag{C1}$$

where $T_\Delta = (T - T_0)/T_0$ and T_0 is the room temperature. In Refs. [5,49], inspired by the Clausius-Mossotti relation, the dielectric ratio

$$\rho(T_\Delta, \omega) = \frac{\epsilon(T_\Delta, \omega) - 1}{\epsilon(T_\Delta, \omega) + 2} \doteq f(T_\Delta, \omega) \tag{C2}$$

was fitted to a functional form corresponding to the master function. That is to say, one fits

$$\epsilon_{\mathrm{CM}}(T_\Delta, \omega) \doteq \frac{1 + 2f(T_\Delta, \omega)}{1 - f(T_\Delta, \omega)}. \tag{C3}$$

We now take the opportunity to correct two unfortunate typographical errors in Ref. [13], Equation (8) of Ref. [13] misses an opening curly parenthesis in the numerator,

$$\rho(T_\Delta, \omega) = \sum_{k=1}^{k_{\max}} \frac{a_k^{\mathrm{CM}}(T_\Delta)\,\big\{\big[\,\omega_k^{\mathrm{CM}}(T_\Delta)\big]^2 - \mathrm{i}\,\gamma_k'^{\mathrm{CM}}(T_\Delta)\,\omega\big\}}{\big[\omega_k^{\mathrm{CM}}(T_\Delta)\big]^2 - \omega^2 - \mathrm{i}\,\omega\,\gamma_k^{\mathrm{CM}}(T_\Delta)}, \tag{C4}$$

while Eq. (9) of Ref. [13] has a typographical error in the last term of the numerator; one needs to replace $\omega^4 \to [\omega_k^{\mathrm{CM}}(T_\Delta)]^4$,

$$\mathrm{Re}[\rho_{\mathrm{CM}}(T_\Delta, \omega)] = \sum_{k=1}^{k_{\max}} a_k^{\mathrm{CM}}(T_\Delta) \frac{\omega^2\big\{\gamma_k^{\mathrm{CM}}(T_\Delta)\,\gamma_k'^{\mathrm{CM}}(T_\Delta) - \big[\omega_k^{\mathrm{CM}}(T_\Delta)\big]^2\big\} + \big[\omega_k^{\mathrm{CM}}(T_\Delta)\big]^4}{\big\{\omega^2 - \big[\omega_k^{\mathrm{CM}}(T_\Delta)\big]^2\big\}^2 + \omega^2\,\big[\gamma_k^{\mathrm{CM}}(T_\Delta)\big]^2}, \tag{C5}$$

while the imaginary part is

$$\mathrm{Im}[\rho_{\mathrm{CM}}(T_\Delta, \omega)] = \sum_{k=1}^{k_{\max}} a_k^{\mathrm{CM}}(T_\Delta)\,\omega \frac{\omega^2\gamma_k'^{\mathrm{CM}}(T_\Delta) + \big\{\gamma_k^{\mathrm{CM}}(T_\Delta) - \gamma_k'^{\mathrm{CM}}(T_\Delta)\big\}\big[\omega_k^{\mathrm{CM}}(T_\Delta)\big]^2}{\big\{\omega^2 - \big[\omega_k^{\mathrm{CM}}(T_\Delta)\big]^2\big\}^2 + \omega^2\big[\,\gamma_k^{\mathrm{CM}}(T_\Delta)\,\big]^2}. \tag{C6}$$

We note that the imaginary part of the dielectric function should be strictly positive for real, positive frequencies, due to causality (see Chap. 6 of Ref. [50]). The region near $\omega \approx 0$ of the CM fit for the imaginary part of $\mathrm{Im}[\epsilon(\omega)]$ has a positive second derivative. This means that, between the frequency points $\omega = 0$ and $\omega = \omega_{\min}$, where $\omega_{\min}$ is the smallest frequency for which the dielectric function has been measured, one has a "gap" where any fitting function runs the risk of "undershooting" the line $\mathrm{Im}[\epsilon(\omega)] = 0$, and the positive second derivative compensates a negative first derivative at $\omega = 0$ to match the points of smallest frequency of the fit.

Indeed, the fitting parameters that were given in Ref. [13] led to spurious negative imaginary parts under some circumstances, but these were so small as to be statistically insignificant [less than 0.2% of the total $\epsilon(\omega)$]. Table I gives the best CM fitting parameters at room temperature, where some entries were slightly adjusted compared to the values given in Ref. [13] (but still within the error bars of the fit) to ensure overall positivity of $\mathrm{Im}[\epsilon(\omega)]$. Figure 7 shows $\epsilon(i\omega)$,

TABLE I. Parameters for the CM fit are indicated for the real parts and for the imaginary parts of the dielectric function for silicon, as given in Eqs. (C5) and (C6), at room temperature ($T_\Delta = 0$ in the notation of Ref. [13]). Here, $a_{1,2}$ are dimensionless and $\omega_{1,2}$, $\gamma_{1,2}$, and $\gamma'_{1,2}$ are in units of $E_h/\hbar$. The values are adapted from Tables I and II of Ref. [13], with minor adjustments of the entries marked by * (see text).

k	a_k	ω_k	γ_k	γ'_k
1	0.004943	0.1293	0.01841	0.1306
2	0.7709	0.3117	0.101*	0.0968*

comparing the adjusted CM fitting parameters of Table I with the original parameters of Ref. [13]. The two curves are essentially on top of each other, with a maximal difference of 0.6%.

APPENDIX D: TRK SUM RULE FOR METASTABLE STATES

The TRK sum rule [11,12] is instrumental in deriving the correct asymptotic form of the dynamic polarizability at large imaginary frequency. It states that the sum over all oscillator strengths is equal to the number of electrons Z of the atom. According to Eq. (61.1) of Ref. [51], it is valid for an arbitrary (e.g., metastable) reference state $|\psi_m\rangle$,

$$\sum_n f_{nm} = Z, \tag{D1}$$

where n sums over all quantum numbers of the system (not just the principal ones). This is confirmed in Eq. (22) of Ref. [52] for excited singlet and triplet reference states which are embedded in a continuum. When comparing to Ref. [52], one notes that the authors of Ref. [52] use, in some parts of

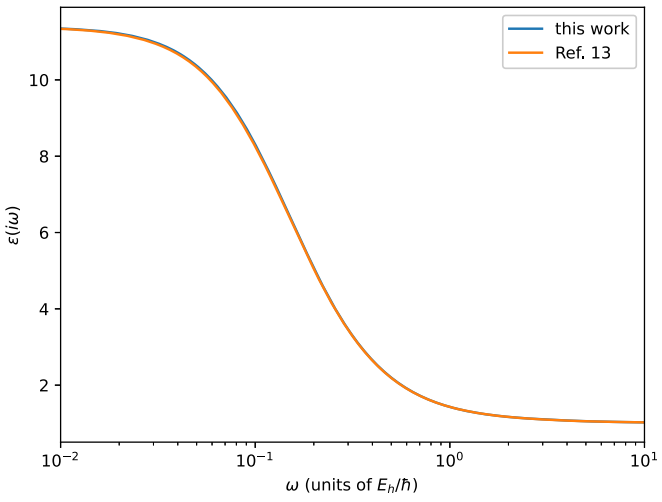

FIG. 7. Dielectric function of silicon at room temperature for the imaginary frequency argument, $\epsilon(i\omega)$. The two curves compare the CM fit using the parameters of Ref. [13] and the adjusted parameters of Table I. The abscissa indicates the angular frequency in atomic units, i.e., the numerical value of $\hbar\omega/E_h$, where E_h is the Hartree energy.

their investigations, a somewhat nonstandard redefinition of the oscillator strengths, adapted to different magnetic projections. Here, we adopt the standard definition of the oscillator strength, which entails an average over the magnetic projections of the reference state $|m\rangle$, and a summation over the magnetic projections of the virtual state $|n\rangle$ (see Sec. 5.5.3 of Refs. [4,53]). In view of the relation

$$\alpha(i\omega) = \sum_n \frac{f_{nm}}{\omega_{nm}^2 + \omega^2}, \tag{D2}$$

the TRK sum rule determines the asymptotic behavior of the polarizability for large ω (the energy difference in atomic units of the virtual state and the reference state is $\omega_{nm} = \omega_n - \omega_m$). Here, we present a derivation which, in contrast to Eq. (11.10) of Ref. [54], is valid for a system with an arbitrary number Z of electrons and for an arbitrary reference state. The Hamiltonian is

$$H = \sum_a \left(\frac{\vec{p}_a^{\,2}}{2} - \frac{Z}{r_a} \right) + \sum_{a<b} \frac{1}{r_{ab}}, \tag{D3}$$

where a and b sum over the electrons, r_a is the electron-nucleus distance, and r_{ab} is the interelectron distance. Indices $a, b, c, d \in \{1, \ldots, Z\}$ enumerate the bound electrons. The (dipole) oscillator strength for the excitation to the states $|\psi_n\rangle$ is

$$f_{nm} = \frac{2}{3} (E_n - E_m) \left| \langle \psi_n | \sum_c \vec{r}_c | \psi_m \rangle \right|^2, \tag{D4}$$

where we re-emphasize the average over the magnetic projections of the reference state $|m\rangle$ and a summation over the magnetic projections of the virtual state $|n\rangle$. The sum over oscillator strengths can be written as follows, in operator notation,

$$\sum_n f_{nm} = \frac{2}{3} \langle \psi_m | \left(\sum_c \vec{r}_c \right) (H - E_m) \left(\sum_d \vec{r}_d \right) | \psi_m \rangle, \tag{D5}$$

where the sum over n includes the continuum. We now make use of the well-known operator identity

$$ABA = \tfrac{1}{2} A^2 B + \tfrac{1}{2} BA^2 + \tfrac{1}{2} [A, [B, A]], \tag{D6}$$

where $A = \sum_c \vec{r}_c$ and $B = H - E_m$. Because $|\psi_m\rangle$ is an eigenstate of the Hamiltonian, we have $(H - E_m)|\psi_m\rangle = 0$ and thus

$$\begin{aligned} \sum_n f_{nm} &= \frac{1}{3} \langle \psi_m | \left[\sum_c \vec{r}_c, \left[H - E_m, \sum_d \vec{r}_d \right] \right] | \psi_m \rangle \\ &= -\frac{i}{3} \langle \psi_m | \left[\sum_c \vec{r}_c, \sum_d \vec{p}_d \right] | \psi_m \rangle \\ &= -\frac{i}{3} \langle \psi_m | \sum_c [\vec{r}_c, \vec{p}_c] | \psi_m \rangle = Z. \end{aligned} \tag{D7}$$

This derivation confirms that the TRK sum rule remains valid for metastable excited states and justifies our parameters for the single-oscillator model of the dynamic polarizability of metastable triplet helium, used in Sec. III. Recently, generalizations of the TRK sum rule suitable for the treatment

of dipole recoil terms which occur in recoil-induced contributions to the shake-off probability following β decay have been discussed in Ref. [55]. Other generalizations with respect to multipole polarizabilities have been considered [56,57]. Their derivation follows the ideas underlying the above considerations.

[1] R. H. French, V. A. Parsegian, R. Podgornik, R. F. Rajter, A. Jagota, J. Luo, D. Asthagiri, M. K. Chaudhury, Y.-M. Chiang, S. Granick, S. Kalinin, M. Kardar, R. Kjellander, D. C. Langreth, J. Lewis, S. Lustig, D. Wesolowski, J. S. Wettlaufer, W.-Y. Ching, M. Finnis *et al.*, Long range interactions in nanoscale science, Rev. Mod. Phys. **82**, 1887 (2010).

[2] L. M. Woods, D. A. R. Dalvit, A. Tkatchenko, P. Rodriguez-Lopez, A. W. Rodriguez, and R. Podgornik, Materials perspective on Casimir and van der Waals interactions, Rev. Mod. Phys. **88**, 045003 (2016).

[3] V. B. Berestetskii, E. M. Lifshitz, and L. P. Pitaevskii, *Quantum Electrodynamics*, 2nd ed., Volume 4 of the Course on Theoretical Physics (Pergamon, Oxford, England, 1982).

[4] U. D. Jentschura and G. S. Adkins, *Quantum Electrodynamics: Atoms, Lasers and Gravity* (World Scientific, Singapore, 2022).

[5] G. Łach, M. DeKieviet, and U. D. Jentschura, Multipole effects in atom-surface interactions: A theoretical study with an application to He–α-quartz, Phys. Rev. A **81**, 052507 (2010).

[6] M. Antezza, L. P. Pitaevskii, and S. Stringari, Effect of the Casimir-Polder force on the collective oscillations of a trapped Bose-Einstein condensate, Phys. Rev. A **70**, 053619 (2004).

[7] U. D. Jentschura, Revisiting the divergent multipole expansion of atom–surface interactions: Hydrogen and positronium, α-quartz, and physisorption, Phys. Rev. A **109**, 012802 (2024).

[8] A. O. Caride, G. L. Klimchitskaya, V. M. Mostepanenko, and S. I. Zanette, Dependences of the van der Waals atom-wall interaction on atomic and material properties, Phys. Rev. A **71**, 042901 (2005).

[9] M. Bordag, G. L. Klimchitskaya, U. Mohideen, and V. M. Mostepanenko, *Advances in the Casimir Effect* (Oxford University, Oxford, England, 2009).

[10] V. Druzhinina and M. DeKieviet, Experimental observation of quantum reflection far from threshold, Phys. Rev. Lett. **91**, 193202 (2003).

[11] F. Reiche and W. Thomas, Über die Zahl der Dispersionselektronen, die einem stationären Zustand zugeordnet sind, Z. Phys. **34**, 510 (1925).

[12] W. Kuhn, Über die Gesamtstärke der von einem Zustande ausgehenden Absorptionslinien, Z. Phys. **33**, 408 (1925).

[13] C. Moore, C. M. Adhikari, T. Das, L. Resch, C. A. Ullrich, and U. D. Jentschura, Temperature-dependent dielectric function of intrinsic silicon: Analytic models and atom-surface potentials, Phys. Rev. B **106**, 045202 (2022).

[14] V. I. Korobov and S. V. Korobov, Bethe logarithm for the $1\,^1S$ and $1\,^1S$ states of helium, Phys. Rev. A **59**, 3394 (1999).

[15] V. I. Korobov, Coulomb three-body bound-state problem: Variational calculations of nonrelativistic energies, Phys. Rev. A **61**, 064503 (2000).

[16] V. I. Korobov, Nonrelativistic ionization energy for the helium ground state, Phys. Rev. A **66**, 024501 (2002).

[17] L. Piela, *Ideas of Quantum Chemistry* (Elsevier, Amsterdam, 2013).

[18] See https://julialang.org.

[19] I. Balbaert, *Getting Started with Julia Programming* (Packt Publishing, Birmingham, England, 2015).

[20] J. Bezanson, A. Edelman, S. Karpinski, and V. B. Shah, Julia: A fresh approach to numerical computing, SIAM Rev. **59**, 65 (2017).

[21] J. H. Noble, M. Lubasch, J. Stevens, and U. D. Jentschura, Diagonalization of complex symmetric matrices: Generalized householder reflections, iterative deflation and implicit shifts, Comput. Phys. Commun. **221**, 304 (2017).

[22] W. L. Wiese and J. R. Fuhr, Accurate atomic transition probabilities for hydrogen, helium, and lithium, J. Phys. Chem. Ref. Data **38**, 565 (2009).

[23] J. F. Babb, G. L. Klimchitskaya, and V. M. Mostepanenko, Casimir-Polder interaction between an atom and a cavity wall under the influence of real conditions, Phys. Rev. A **70**, 042901 (2004).

[24] P. Schwerdtfeger and J. K. Nagle, 2018 Table of static dipole polarizabilities of the neutral elements in the periodic table, Mol. Phys. **117**, 1200 (2019).

[25] R. Brühl, P. Fouquet, R. E. Grisenti, J. P. Toennies, G. C. Hegerfeldt, T. Köhler, M. Stoll, and C. Walter, The van der Waals potential between metastable atoms and solid surfaces: Novel diffraction experiments versus theory, Europhys. Lett. **59**, 357 (2002).

[26] K. T. Tang, Dynamic polarizabilities and van der Waals coefficients, Phys. Rev. **177**, 108 (1969).

[27] A. Kramida, Y. Ralchenko, and J. Reader, NIST ASD Team (2020). NIST Atomic Spectra Database (version 5.8), online, available at https://physics.nist.gov/asd (Fri. Sept. 10 2021), National Institute of Standards and Technology, Gaithersburg, MD, https://doi.org/10.18434/T4W30F.

[28] U. D. Jentschura and C. Moore, Logarithmic terms in atom-surface potentials: Limited applicability of rational approximations for intermediate distance, Phys. Rev. A **108**, 012815 (2023).

[29] E. D. Palik, *Handbook of Optical Constants of Solids* (Academic Press, San Diego, 1985).

[30] G. W. Erickson and D. R. Yennie, Radiative level shifts, I. Formulation and lowest order Lamb shift, Ann. Phys. (NY) **35**, 271 (1965).

[31] G. W. Erickson and D. R. Yennie, Radiative level shifts, II. Higher order contributions to the Lamb shift, Ann. Phys. (NY) **35**, 447 (1965).

[32] G. W. Erickson, Improved Lamb-shift calculation for all values of Z, Phys. Rev. Lett. **27**, 780 (1971).

[33] J. Sapirstein, Higher-order binding corrections to the Lamb shift, Phys. Rev. Lett. **47**, 1723 (1981).

[34] K. Pachucki, Higher-order binding corrections to the Lamb shift, Ann. Phys. (NY) **226**, 1 (1993).

[35] U. D. Jentschura, P. J. Mohr, and G. Soff, Calculation of the electron self-energy for low nuclear charge, Phys. Rev. Lett. **82**, 53 (1999).

[36] H. Hoinkes, The physical interaction potential of gas atoms is with single-crystal surfaces, determined from gas-surface diffraction experiments, Rev. Mod. Phys. **52**, 933 (1980).
[37] E. Zaremba and W. Kohn, Van der Waals interaction between an atom and a solid surface, Phys. Rev. B **13**, 2270 (1976).
[38] J. Tao and A. M. Rappe, Physical Adsorption: Theory of van der Waals interactions between particles and clean surfaces, Phys. Rev. Lett. **112**, 106101 (2014).
[39] P. L. Silvestrelli, A. Ambrosetti, S. Grubisiĉ, and F. Ancilotto, Adsorption of rare-gas atoms on Cu(111) and Pb(111) surfaces by van der Waals corrected density functional theory, Phys. Rev. B **85**, 165405 (2012).
[40] S. Grimme, J. Antony, S. Ehrlich, and H. Krieg, A consistent and accurate *ab initio* parametrization of density functional dispersion correction (DFT-D) for the 94 elements H-Pu, J. Chem. Phys. **132**, 154104 (2010).
[41] D. T. Aznabaev, A. K. Bekbaev, and V. I. Korobov, Nonrelativistic energy levels of helium atoms, Phys. Rev. A **98**, 012510 (2018).
[42] V. A. Yerokhin, V. Patkoś, and K. Pachucki, Atomic structure calculations of helium with correlated exponential functions, Symmetry **13**, 1246 (2021).
[43] G. W. F. Drake and Z. C. Yan, Energies and relativistic corrections for the Rydberg states of helium: Variational results and asymptotic analysis, Phys. Rev. A **46**, 2378 (1992).
[44] Z.-C. Yan and J. F. Babb, Long-range interactions of metastable helium atoms, Phys. Rev. A **58**, 1247 (1998).
[45] G. W. F. Drake, High precision theory of atomic helium, Phys. Scr. T **83**, 83 (1999).
[46] G. W. F. Drake, High precision calculations for helium, in *Springer Handbook of Atomic, Molecular, and Optical Physics* (Springer, New York, 2005).
[47] K. Pachucki and J. Sapirstein, Relativistic and QED corrections to the polarizability of helium, Phys. Rev. A **63**, 012504 (2000).
[48] A. W. Weiss, Oscillator strengths for the helium isoelectronic sequence, J. Res. Natl. Bur. Stand., Sect. A **71**, 163 (1967).
[49] K. E. Oughstun and N. A. Cartwright, On the Lorentz-Lorenz formula and the Lorentz model of dielectric dispersion, Opt. Express **11**, 1541 (2003).
[50] U. D. Jentschura, *Advanced Classical Electrodynamics: Green Functions, Regularizations, Multipole Decompositions* (World Scientific, Singapore, 2017).
[51] H. A. Bethe and E. E. Salpeter, *Quantum Mechanics of One- and Two-Electron Atoms* (Springer, Berlin, 1957).
[52] G. W. F. Drake and A. Dalgarno, $2p^2\,{}^3P$ and $2p3p\,{}^1P$ states of the helium isoelectronic sequence, Phys. Rev. A **1**, 1325 (1970).
[53] R. C. Hilborn, Einstein coefficients, cross sections, f values, dipole moments, and all that, Am. J. Phys. **50**, 982 (1982).
[54] H. A. Bethe and R. Jackiw, *Intermediate Quantum Mechanics* (Perseus, New York, 1986).
[55] E. E. Schulhoff and G. W. F. Drake, Electron emission and recoil effects following the beta decay of ^{6}He, Phys. Rev. A **92**, 050701(R) (2015).
[56] Z.-C. Yan, J.-M. Zhu, and B.-L. Zhou, Polarizabilities of heliumlike ions in the $1s2p\,{}^1P$ and $1s2p\,{}^3P$ states, Phys. Rev. A **62**, 034501 (2000).
[57] B.-L. Zhou, J.-M. Zhu, and Z.-C. Yan, Generalized Thomas-Reiche-Kuhn sum rule, Phys. Rev. A **73**, 014501 (2006).